Introduction of the Pre-calibration Package GEO-TRACE-PAK: An Analytical Package for Trace Elements Including Rare Earth Elements in Rocks

Yasujiro Yamada*

Abstract

X-ray fluorescence (XRF) spectrometry enables the rapid, nondestructive analysis of a wide range of different sample types. However, as it is a relative analytical method, quantitative analysis requires preparing standard samples, establishing calibration curves, and optimizing correction conditions, which results in longer analysis times and higher costs. This report describes the features and effectiveness of "GEO-TRACE-PAK," a pre-calibration analytical package specifically designed for analyzing trace elements, including rare earth elements, in rocks. To validate this package, which includes optimized measurement conditions and correction settings based on approximately 110 standard samples, multiple geological reference materials were analyzed. The results demonstrated good agreement with reported reference and literature values for the constituent elements. GEO-TRACE-PAK is expected to be an effective and practical method for geological sample analysis, enabling the immediate analysis of test samples without the need for additional standard samples.

1. Introduction

X-ray fluorescence (XRF) spectrometry enables rapid, nondestructive, and highly precise analysis of the elemental composition of a wide range of samples. Therefore, this method is widely applied in the research and development of new materials across various fields and for quality control in manufacturing processes. However, XRF quantitative analysis can be time-consuming and costly because it is a relative quantitative method: to obtain accurate results, the user must prepare multiple standard materials, which can be expensive, and must also determine suitable measurement conditions and configure appropriate correction methods (e.g., matrix corrections for absorption and enhancement effects and line-overlap corrections) even when such standards are available.

Rigaku offers analytical application packages for routine analyses, including Quantitative Application Packages and Pre-Calibration Packages. Each Quantitative Application Package includes physical standards and drift-correction samples. Before analysis, the user installs the analytical parameters (measurement conditions, standard sample information, and various corrections), measures appropriately prepared standard samples, creates and registers calibration curves using the acquired X-ray intensity data, and registers drift-correction samples to maintain instrument sensitivity.

In contrast, each Pre-Calibration Package does not include physical standard samples. Instead, the user installs the provided analytical parameters (measurement conditions, standard sample information, calibration constants, and various corrections) and then measures the included drift-correction sample (a stable glass specimen). This procedure completes the setup for both the calibration curves and the drift-correction parameters for sensitivity. There is no need to purchase expensive standard samples, allowing test samples to be analyzed immediately after the instrument is installed.

This report introduces GEO-TRACE-PAK, a Pre-Calibration Package specifically designed for analyzing trace elements, including rare earths, in rocks, for use with Rigaku ZSX Primus IV, ZSX Primus IVi, and ZSX Primus III NEXT spectrometers.

2. Introduction to GEO-TRACE-PAK

2.1. Features

The Pre-Calibration Package GEO-TRACE-PAK[1] is designed for the quantitative analysis of powder samples. It was developed based on approximately 110 standard materials, primarily oxides such as rocks, soils, ores, and minerals. This package comes with pre-integrated analytical conditions, calibration parameters, and correction factors, enabling the analysis of 37 trace elements. Additionally, it includes eight major components as reference values for matrix corrections. Long-term maintenance of the calibration curves can be achieved using drift-correction parameters established from measurements of the glass sample supplied.

Even samples with poor formability can be prepared for measurement by mixing with a specified binder and molding under pressure. The binder mixing ratio is entered as an input parameter in the software, so it does not need to be fixed and can flexibly accommodate a range of compositions (with the binder content up to 10 wt% of the total sample weight).

* Product Division XRF WDX Group, Rigaku Corporation.

Table 1. List of Standard Reference Materials (Rocks, Soils, and Ores)

GSJ		
No.	S. name	Rock type
1	JA-1	Andesite
2	JA-2	Andesite
3	JA-3	Andesite
4	JB-1a	Basalte
5	JB-1b	Basalte
6	JB-2	Basalte
7	JB-3	Basalte
8	JG-1a	Granite
9	JG-2	Granite
10	JG-3	Granite
11	JGb-1	Gabbro
12	JR-1	Rhyolite
13	JR-2	Rhyolite
14	JR-3	Rhyolite
15	JH-1	Hornblendite
16	JMS-1	Marine Sediment
17	JMS-2	Marine Sediment
18	JF-1	Feldspar
19	JF-2	Feldspar
20	JDo-1	Dolomite
21	JP-1	Peridotite
22	JSy-1	Synite
23	JSl-1	Slate
24	JSO-1	Black forest soil
25	JSO-2	Soil
26	JSd-1	Sediment
27	JSd-2	Sediment
28	JSd-3	Sediment
29	JSd-4	River Sediment
30	JLk-1	Lake sediment
31	JLs-1	Limestone
32	JCu-1	Cu ore
33	JZn-1	Zn ore

USGS		
No.	S. name	Rock type
34	AVG-2	Andesite
35	BCR-2	Basalte
36	BHVO-2	Basalte
37	BIR-1	Basalte
38	BIR-1a	Basalte
39	COQ-1	Carbonatite
40	DNC-1	Dolerite
41	DNC-1a	Dolerite
42	DTS-2b	Dunite
43	GSP-2	Granodiorite
44	GXR-1	Jasperoid
45	MAG-1	Sediment
46	QLO-1a	Quartz
47	SCo-1	Shale
48	SDC-1	Mica
49	SGR-1	Shale
50	SGR-1b	Shale
51	STM-1	Syenite
52	STM-2	Syenite
53	W-2a	Diabase
54	RGM-1	Rhyolite
55	RGM-2	Rhyolite

CANMET		
No.	S. name	Rock type
56	SY-2	Syenite
57	SY-3	Syenite
58	SY-4	Diolite
59	MRG-1	Gabbro
60	FER-2	Iron formation
61	FER-3	Iron formation
62	FER-4	Iron formation
63	UM-2	Ultra magnific
64	HISS-1	Marine Sediment
65	MESS-2	Estuarine Sediment
66	PACS-2	Marine Sediment
67	BH-1	W ore
68	CH-1	W ore
69	TLG-1	W ore

MINTEK		
No.	S. name	Rock type
70	NIM-G	Granite
71	NIM-S	Synite
72	NIM-L	Lujavrite
73	NIM-N	Norite
74	NIM-P	Pyroxenite

NRCGA		
No.	S. name	Rock type
75	GSO-Cu-1	Cu ore
76	GSO-Cu-1	Cu ore
77	GSO-Pb-1	Pb ore
78	GSO-Pb-2	PC ore
79	GSO-Zn-1	Zn ore
80	GSO-Mo-1	Mo ore
81	GSO-Mo-2	Mo ore
82	GSO-W-1	W ore
83	GSO-W-2	W ore

IGGE		
No.	S. name	Rock type
84	GSR-1	Granite
85	GSR-2	Andesite
86	GSR-4	Stream sediment
87	GSR-5	Shale
88	GSR-6	Carbonate
89	GSR-7	Syenite
90	GSR-9	Diolite
91	GSR-10	Gabbro
92	GSR-11	Rhyolite
93	GSD-2	Stream sediment
94	GSD-4	Stream sediment
95	GSD-6	Stream sediment
96	GSD-9	Sediment
97	GSD-11	Sediment
98	GSS-1	Soil
99	GSS-3	Soil
100	GSS-5	Soil
101	GSS-7	Soil
102	CJ-1	China Loess

NIST		
No.	S. name	Rock type
103	1646a	Estuarine Sediment
104	2709	San Joaquin soil
105	2709a	San Joaquin soil
106	2710	Montana I soil
107	2710a	Montana I soil
108	2711	Montana II soil
109	2711a	Montana II soil
110	8704	Buffalo River Sediment

NIES		
No.	S. name	Rock type
111	NIES2	Pond Sediment

Sample Source	
GSJ:	Geological Survey of Japan
USGS:	United States Geological Survey
CANMET:	Canadian Certificated Reference Materials Project
MINTEK:	National Institute for Metallurgy
NRCGA:	National Reseach Center of Geoanalysis
IGGE:	Institute of Geophysical and Geochemical Exploration
NIST:	National Institute of Standards and Technology
NIES:	National Institute for Environmental Studies

2.2. Elements and Compounds for Measurement

The updated version of GEO-TRACE-PAK (Version2) can analyze additional trace elements, including rare earth elements.

The target elements and compounds are listed below. Note that some major components (excluding Al_2O_3 and SiO_2) are included as references for matrix corrections. The newly added analytical targets are underlined.

- Trace Elements (including rare-earth elements)
  F, Sc, V, Cr, Mn, Co, Ni, Cu, Zn, Ga, Ge, As, Br, Rb, Sr, Y, Zr, Nb, Mo, Ag, Cd, Sn, Sb, Ba, La, Ce, Pr, Nd, Sm, Eu, Yb, Hf, W, Pb, Bi, Th, and U.
- Major Components (as references)
  Na_2O, MgO, P_2O_5, S, K_2O, CaO, TiO_2, and Fe_2O_3

2.3. List of Standard Reference Materials Used

All standard materials listed in Table 1 were used to establish the calibration curves. These consist of approximately 110 standard materials from various sources, including igneous rocks, limestones, sediments, and ores (copper, lead, zinc, molybdenum, tungsten, etc.).

2.4. Optimization of Optical Conditions

The selection of optical conditions has a significant impact on analytical precision in trace elements, particularly in the heavy-element region (energies at or above the Ti–K line). The key considerations for these settings are as follows:

a) Optimizing background angles to minimize interference from overlapping lines.
b) Selecting optical conditions that minimize the influence of interfering lines on the analytical lines.
c) Improving the lower limit of detection (LLD) by selecting appropriate primary X-ray filters to enhance the peak-to-background (P/B) ratio.

Table 2 lists the primary X-ray filters, analyzing

Table 2. List of Primary X-ray Filters, Analysis Crystals, Detector and Divergent Slits for Each Analytical Line

<table>
<tr><th>Analytical lines for major and correction</th><td colspan="4"></td><td>Rh-Kα Compton</td><td colspan="21"></td><td>Fe-Kα</td><td colspan="9"></td><td>Ti-Kα</td><td colspan="2"></td><td>Ca-Kα</td><td>K-Kα</td><td>S-Kα</td><td>P-Kα</td><td>Mg-Kα</td><td>Na-Kα</td><td></td></tr>
<tr><th>Analytical Lines for trace</th><td>Sb-Kα</td><td>Sn-Kα</td><td>Cd-Kα</td><td>Ag-Kα</td><td></td><td>Mo-Kα</td><td>Nb-Kα</td><td>Zr-Kα</td><td>Y-Kα</td><td>Sr-Kα</td><td>U-Lα</td><td>Rb-Kα</td><td>Th-Lα</td><td>Pb-Lβ1</td><td>Br-Kα</td><td>As-Kβ1</td><td>Bi-Lα</td><td>Ge-Kα</td><td>Ga-Kα</td><td>Zn-Kα</td><td>W-Lα</td><td>Cu-Kα</td><td>Hf-Lα</td><td>Ni-Kα</td><td>Yb-Lα</td><td>Co-Kα</td><td></td><td>Mn-Kα</td><td>Eu-Lα</td><td>Sm-Lα</td><td>Pr-Lβ1</td><td>Cr-Kα</td><td>Ce-Lβ1</td><td>Nd-Lα</td><td>V-Kα</td><td>La-Lα</td><td></td><td>Ba-Lα</td><td>Sc-Kα</td><td colspan="6"></td><td>F-Kα</td></tr>
<tr><th>Primary X-ray Filter</th><td colspan="4">Ni400</td><td>Al25</td><td colspan="14">Ni40</td><td colspan="7">Al125</td><td>Al25</td><td colspan="9">Al125</td><td colspan="5">Al25</td><td colspan="5">Be30 or Out</td></tr>
<tr><th>Analysis Crystal</th><td colspan="34">LiF(220)</td><td colspan="7">LiF(200)</td><td colspan="2">Ge</td><td colspan="3">RX26</td></tr>
<tr><th>Detector</th><td colspan="35">SC</td><td>FPC</td><td colspan="2">SC</td><td colspan="8">FPC</td></tr>
<tr><th>Divergent Slit</th><td colspan="39">S2</td><td>S4</td><td colspan="6">S2</td></tr>
</table>

crystals, and divergent slits employed for each analytical line (trace elements and major components).

A Be30 filter is available as an option and is strongly recommended for tube-below type instruments. For measurements from F-Kα to S-Kα, a Be30 is the only suitable primary X-ray filter for X-ray tube protection. Other standard filters significantly reduce the excitation efficiency for these light elements, making reliable quantitative analysis difficult.

2.4.1. Analysis Crystals and Detectors in the Heavy-Element Region

In trace-element analysis, minimizing line overlaps and optimizing background settings are essential, as noted above. These factors are particularly crucial in the heavy-element region, where the K and L lines from major constituent elements overlap in a complex manner. For heavy-element measurements, LiF(220), with its higher angular resolution compared with LiF(200), is often preferred as the analyzing crystal.

For the same reason, a scintillation counter (SC) combined with a receiving slit is used to enhance angular resolution. This reduces peak overlaps and facilitates the selection of background angles. Although X-ray intensity decreases with increasing angular resolution, sufficient precision can be ensured by extending the measurement time.

Comparative spectra obtained using LiF(220) or LiF(200) crystals are shown in Fig. 1-1, 1-2, and 1-3 (the horizontal axis represents wavelength). As shown in Fig. 1-1, when LiF(220) is used, both the overlap between U-Lα and Rb-Kα is reduced and the background in the indicated region becomes flatter. Figure 1-2 shows that LiF(220) also improves the resolution in the region where Ni-Kα and Yb-Lα lines overlap. Note that it is often essential to optimize the optical conditions to maximize the resolution of Ni lines when analyzing rocks and ores, as these materials typically contain Ni over a wide concentration range, from a few ppm to percent levels.

The selectable LiF crystal must also be chosen with consideration of the detector scanning range. The maximum scanning range of the SC detector is 118° (2θ), which limits the maximum measurable wavelength with LiF(220) to approximately 0.24 nm, near the wavelength of Nd-Lα. Therefore, LiF(200) is used for detecting La-Lα, V-Kα, Ba-Lα, and Sc-Kα, whose wavelengths fall outside the accessible range of LiF(220).

Certain elements require specific combinations of detector, analyzing crystal, and optical configuration to accommodate their respective spectral interferences and sensitivity requirements. Since V-Kα and Ba-Lα are significantly affected by overlap with Ti-Kβ_1 and Ti-Kα, respectively, and Ti is a major component in many rock samples, an SC detector with good angular resolution is employed. In contrast, La-Lα has fewer interfering lines, allowing the use of a gas-flow proportional counter (FPC) to maximize sensitivity. Although the FPC provides lower resolution because of its short

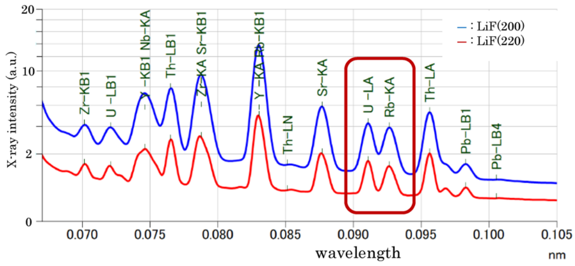

Fig. 1-1. Comparative spectra obtained using LiF(220) or LiF(200) analysis crystals over the wavelength range of 0.070–0.105 nm

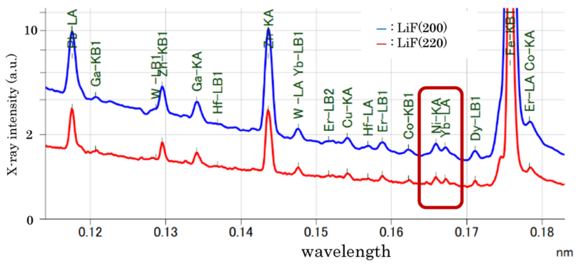

Fig. 1-2. Comparative spectra obtained using LiF(220) or LiF(200) analysis crystals over the wavelength range of 0.120–0.180 nm

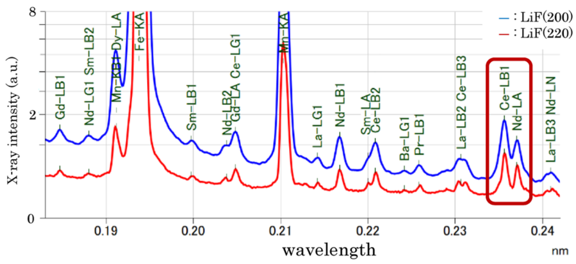

Fig. 1-3. Comparative spectra obtained using LiF(220) or LiF(200) analysis crystals over the wavelength range of 0.185–0.240 nm

Table 3. Selection of Analysis Crystals (LiF(220), LiF(200)) and Detectors (SC, FPC) for Heavy Trace Elements

List of analysis lines and elements applying LiF(200)-SC

Analysis line	Element
Kα	Cr, Mn, Co, Ni, Cu, Zn, Ga, Ge, Br, Rb, Sr, Y, Zr, Nb, Mo, Ag, Cd, Sn, Sb
Kβ_1	As
Lα	Nd, Sm, Eu, Yb, Hf, W, Bi, Th, U
Lβ_1	Ce, Pr, Pb

List of analysis lines and elements applying LiF(200)-SC or LiF(200)-FPC

Analysis line	Detector	Element
Kα	FPC	Sc
	SC	V
Lα	SC	Ba
	FPC	La

receiving-slit length, it offers higher counting efficiency. Sc-Kα is measured using a LiF(200) crystal, an FPC detector, and a high-resolution slit (S2) as the divergent slit to improve peak separation, because the line lies on the tail of the satellite peak adjacent to Ca-Kβ_1 from the major component Ca.

Table 3 shows the analysis lines that are measured utilizing the different combinations of analysis crystals (LiF(220), LiF(200)) and detectors (SC, FPC). A high-resolution divergence slit (S2), which is well-suited to the heavy-element region, is used for all measurements.

For elements measured using their K lines, the Kα line is generally adopted as the analytical line because of its high intensity. The only exception is As, whose Kα line appears at nearly the same position as Pb-Lα. Since rock and ore samples may contain Pb over a wide concentration range from ppm to percent levels, this interference can be significant. Therefore, As-Kβ_1, which is free from Pb interference, is adopted as the analytical line.

For elements using L lines, the intensities of Lα and Lβ_1 line are generally comparable Therefore, the analytical line was selected primarily on the basis of spectral interference from major components and the background profile. For example, for Sm, Sm-Lβ_1 is located at the tail of the Fe-Kα peak of Fe, a major rock component (Fig. 1-3). Accurate determination of the Sm net intensity can be challenging, especially for samples with the Fe_2O_3 content varying from approximately 0.1% to several tens of percent, because of the difficulty in determining the background slope associated with Fe-Kα peak. Thus, Sm-Lα, which has less interference, is used as the analytical line.

For Ce, Ce-Lβ_1 is selected to avoid interference from Ba-Lβ_1 that affects Ce-Lα. Similarly, Pr-Lβ_1 is adopted for Pr measurements as Pr-Lα overlaps with La-Lβ_1.

2.4.2. Use of Primary X-ray Filters

Primary X-ray filters are placed between the X-ray tube and the sample to selectively remove characteristic and continuous X-rays emitted from the X-ray tube. This prevents interference when tube-emitted characteristic X-rays overlap with the analytical lines, thereby enabling a higher peak-to-background (P/B) ratio and a lower LLD by reducing the background. This effect is particularly beneficial for trace-element analysis in the heavy-element region. Therefore, it is crucial to select an appropriate X-ray filter based on the specific analytical conditions. Table 4 shows the combinations of various primary X-ray filters and analytical lines in the heavy-element region.

Table 4. Combinations of Various Primary X-ray Filters and Analysis Lines in the Heavy-Element Region

Primary X-ray filter	Applied analytical line
Ni400	Ag-Kα, Cd-Kα, Sn-Kα, Sb-Kα
Ni40	Ga-Kα, Ge-Kα, As-Kβ_1, Br-Kα, Rb-Kα, Sr-Kα, Y-Kα Zr-Kα, Nb-Kα, Mo-Kα Pb-Lβ_1, Bi-Lα, Th-Lα, U-Lα
Al125	Cr-Kα, V-Kα, Mn-Kα, Co-Kα, Ni-Kα, Cu-Kα, Zn-Kα La-Lα, Ce-Lβ_1, Pr-Lβ_1, Nd-Lα, Sm-Lα, Eu-Lα, Yb-Lα Hf-La, W-Lα
Al25	Ba-Lα, Sc-Kα

Applications:

- Ni400: Removal of characteristic X-rays and Compton scattering lines from the Rh X-ray tube; improvement of the P/B ratio near the maximum intensity of continuous X-rays
- Ni40: Reduction of continuous X-rays and improvement of the P/B ratio in the K-line region for Ga–Mo and the L-line region for Pb–U
- Al125: Reduction of continuous X-rays and improvement of the P/B ratio in the K-line region for Cr–Zn and the L-line region for La–Yb
- Al25: X-ray tube protection filter. Applied when Ni400, Ni40, or Al125 are not used in energy regions above K-Kα

Table 4 lists the combinations of primary X-ray filters and analytical lines used in GEO-TRACE-PAK.

The following list presents representative examples demonstrating the application of primary X-ray filters (Ni400, Ni40, and Al125).

〈Case Study for Ni400: Cd-Kα (Removal of Characteristic X-rays)〉

The Rh-Kβ_2 line emitted from the Rh X-ray tube overlaps with Cd-Kα and can significantly affect Cd determination. A Ni400 filter is therefore used to eliminate this interference. Figure 2-1 compares the Cd-Kα spectra of a sample containing 38 ppm Cd with those of a blank sample containing 0.07 ppm Cd (below the LLD), both measured using the Ni400 filter. Figure 2-2 shows the Cd-Kα spectra of the same samples measured without the filter.

〈Case Study for Ni400: Sb-Kα (P/B Ratio and LLD Improvement)〉

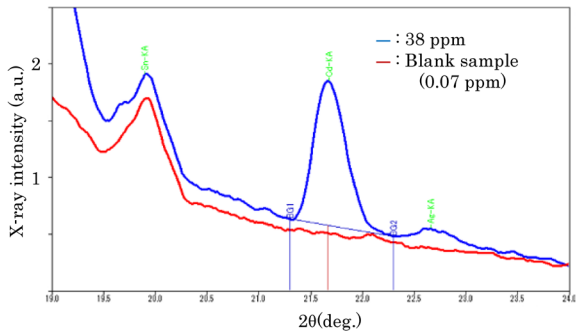

Fig. 2-1. Overlaid Cd-Kα spectra with the Ni400 filter

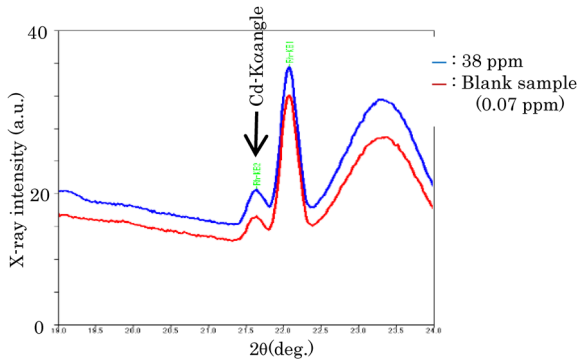

Fig. 2-2. Overlaid Cd-Kα spectra without the Ni400 filter

The effectiveness of the Ni400 filter was evaluated for the Sb-Kα analytical line, which is located near the intensity maximum of the continuous X-ray spectrum. Figure 3-1 and 3-2 show the Sb-Kα spectra of a sample containing 19 ppm Sb measured with and without the Ni400 filter, respectively. With the use of Ni400, the P/B ratio increased significantly from 1.04 to 1.39. Furthermore, the LLD (under the measurement conditions of peak 40 s, BG 20 s × 2) improved from 2.4 to 2.3 ppm, contributing to the enhanced detection sensitivity for trace Sb.

〈Case Study for Ni40: Sr-Kα (P/B Ratio and LLD Improvement)〉

The effectiveness of the Ni40 primary X-ray filter on the analytical line Sr-Kα was evaluated using a sample containing 62 ppm Sr. Figures 4-1 and 4-2 show the Sr-Kα spectra measured with and without the Ni40 filter, respectively. The use of the Ni40 filter dramatically improved the P/B ratio from 2.03 to 5.83 and the LLD from 0.93 to 0.77 ppm (under the measurement conditions of peak 20 s, BG 10 s × 2). These results demonstrate that the Ni40 filter enhances the detection sensitivity for trace Sr.

〈Case Study for Al125: Ce-Lβ_1 (P/B Ratio and LLD Improvement)〉

The effectiveness of the Al125 primary X-ray filter on the analytical line Ce-Lβ_1 was evaluated using a sample containing 327 ppm Ce. Figures 5-1 and 5-2 show the Ce-Lβ_1 spectra measured with and without the Al125 filter, respectively. Application of the Al125 significantly improved the P/B ratio from 1.87 to 4.42 and the LLD from 11 to 8.4 ppm (under the measurement

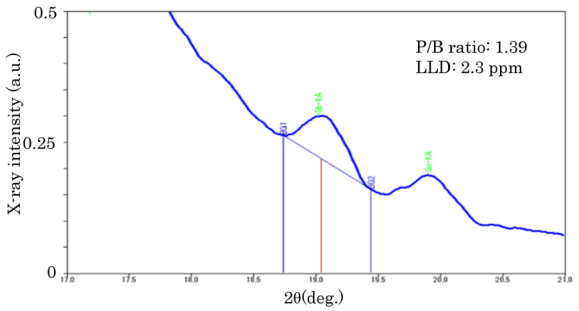

Fig. 3-1. Sb-Kα spectrum (19 ppm Sb) with the Ni400 filter

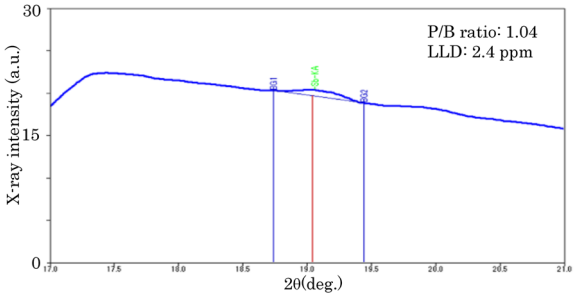

Fig. 3-2. Sb-Kα spectrum (19 ppm Sb) without the Ni400 filter

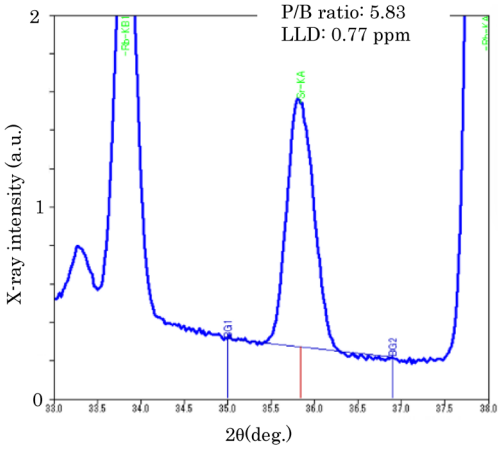

Fig. 4-1. Sr-Kα spectrum (62 ppm Sr) with the Ni40 filter

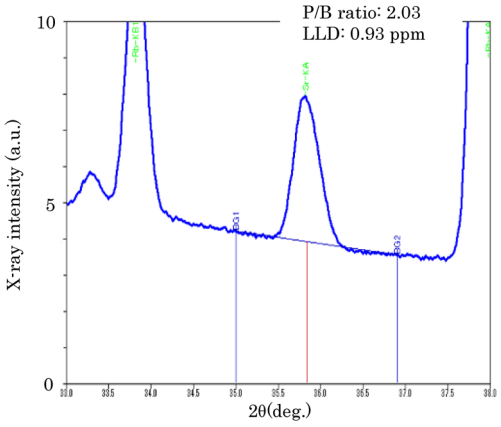

Fig. 4-2. Sr-Kα spectrum (62 ppm Sr) without the Ni40 filter

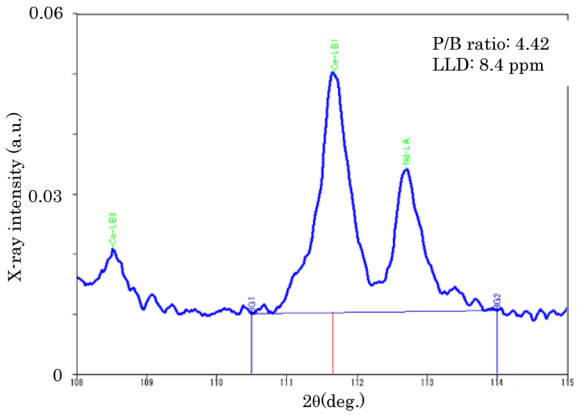

Fig. 5-1. Ce-Lβ_1 spectrum (327 ppm Ce) using the Al125 filter

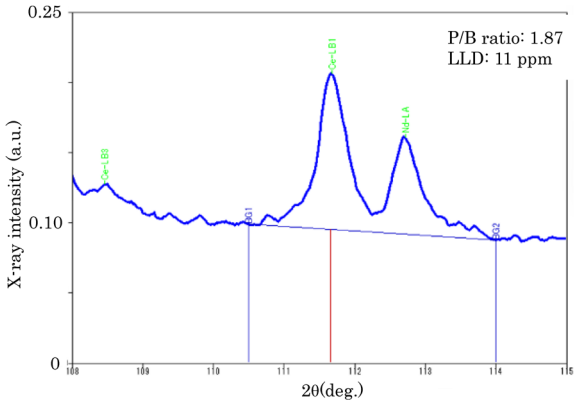

Fig. 5-2. Ce-Lβ_1 spectrum (327 ppm Ce) without the Al125 filter

conditions of peak 200 s, BG 100 s × 2). These results demonstrate that the Al125 effectively enhances the detection sensitivity for trace Ce.

2.4.3 Application of the FPC Detector for Trace Lanthanum Detection

The La-Lα, an analytical line in the heavy-element region used for trace La determination, is relatively less affected by interfering elements than other analysis lines. Therefore, sensitivity rather than resolution can be prioritized, and an FPC detector with superior counting efficiency can be employed to enhance the LLD. Figures 6-1 and 6-2 show the La-Lα spectra of a sample containing 179 ppm of La obtained with the FPC and SC detectors, respectively, using an Al125 filter. The FPC detector significantly improved the P/B ratio from 2.9 to 6.4 and the LLD from 7 to 3.2 ppm (under the measurement conditions peak 200 s, BG 100 s × 2). These results demonstrate that the FPC detector is well suited for high-sensitivity determination of trace La.

2.4.4. Analysis of Trace Fluorine in the Light-Element Region

This package also includes fluorine (F) as a trace analytical target. A primary challenge in the analysis of F in geological samples is the proximity of the Fe-Lα line, originating from Fe, a major constituent of rocks, to the analytical line F-Kα. Consequently, accurate F determination requires effective separation of the Fe-Lα interference.

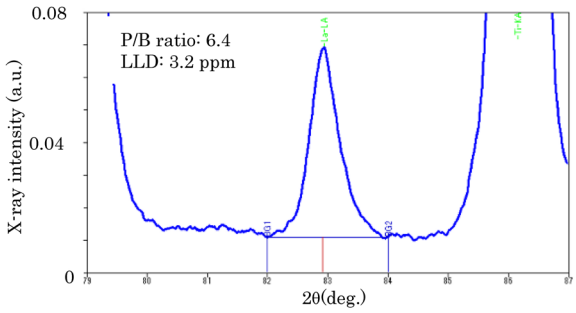

Fig. 6-1. La-Lα spectrum (179 ppm La) using a LiF(200)-FPC detector and Al125 filter

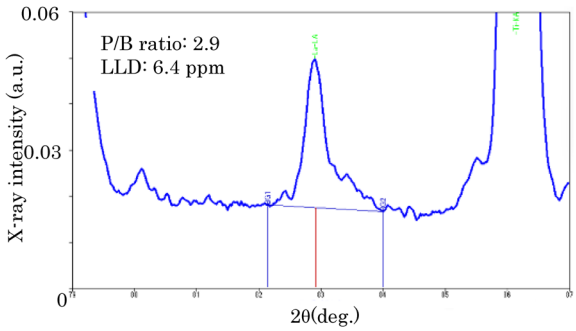

Fig. 6-2. La-Lα spectrum (179 ppm La) using a LiF(200)-SC detector and Al125 filter

The standard analyzer crystal RX26 for light elements ranging from F to Mg is designed to provide high resolution in that region. Its excellent spectral resolution enables measurement of F-Kα while minimizing interference from Fe-Lα. In contrast, the optional RX35 crystal offers approximately four times higher sensitivity than RX26, but its lower spectral resolution causes F-Kα to fall within the tail of the Fe-Lα peak. As a result, overlap corrections can become substantial, particularly for geological samples in which the Fe concentration varies over a wide range, potentially degrading quantitative accuracy.

For these reasons, the RX26 analyzer crystal was selected for F-Kα analysis in this package. Figures 7-1 and 7-2 show the F-Kα spectra for a sample containing 972 ppm F obtained using the RX26 and RX35 crystals, respectively. The spectra demonstrate that RX26 effectively suppresses interference from Fe-Lα, resulting in excellent separation of the F-Kα peak.

2.4.5 Background Position Selection

Accurate determination of the net intensity of an analytical line is indispensable for reliable quantitative analysis. Because the net intensity is directly dependent on the background correction, the selection of appropriate background positions is critically important. In trace-element analysis of rock samples, fluorescent X-rays from other elements frequently overlap the selected background positions. As a result, potential spectral interferences must be carefully evaluated when establishing background positions.

To optimize background positions, spectra from judiciously selected reference samples should be

compared. At a minimum, the evaluation should include the reference samples having:

a) The maximum concentration of the analyte
b) The minimum concentration of the analyte
c) The maximum concentration of an element that may interfere with the analytical line.

The spectra of these standards should be compared using an overlaid plot to verify the background positions.

In addition to the commonly considered K and L lines, some heavy elements exhibit weak fluorescent lines (minor transition lines) arising from minor transitions, such as an M-to-N transition. Although these minor transition lines are often overlooked, they can occur near background positions and should therefore be taken into account during the process of background position selection.

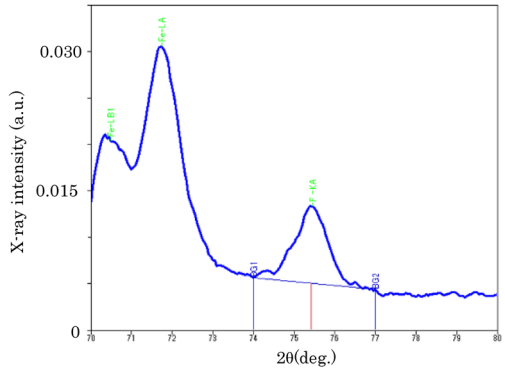

Fig. 7-1. F-Kα spectrum (972 ppm F) using RX26-FPC

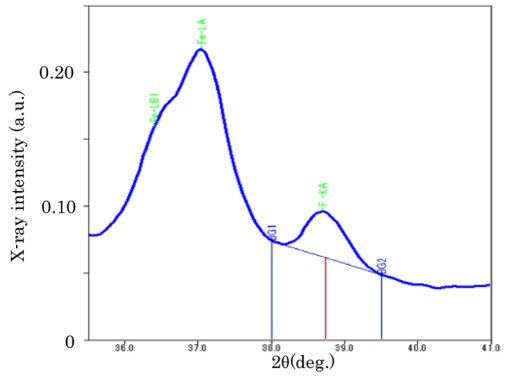

Fig. 7-2. F-Kα spectrum (972 ppm F) using RX35-FPC

Figure 8 presents an example of the interference by minor transition lines that occurred during an analysis of trace Sc using the Sc-Kα line. When analyzing trace Sc in rocks, the elements overlapping Sc-Kα are often Ca-Kβ_1 and its satellite line (Ca-SKβ'), both originating from the major constituent Ca. Accordingly, overlaid spectral plots around the Sc-Kα should be examined using samples containing the maximum and minimum Sc concentrations, as well as the sample containing the maximum Ca concentration, to identify background positions that are unaffected by Ca transition lines.

In some cases, rock samples may contain up to approximately 1000 ppm Th, and its minor transition line Th-M_2–N_4 may occur very close to a candidate background position for Sc-Kα, as shown in Fig. 8. Therefore, care should be taken to avoid such minor transition lines as well. In the case of Sc-Kα, for example, an interference-free region on the low-angle side provides a more suitable background position.

2.5 Matrix Correction

When analyzing the heavy-element region in rocks, it is crucial to properly correct for matrix effects caused by coexisting elements. In particular, the major components of rock samples—Fe_2O_3, TiO_2, CaO, and K_2O—exert significant absorption and excitation effects on the analytical lines. For analytical lines with wavelengths shorter (higher energy) than the Fe-K absorption edge (Fe-K_{abs}), the Compton scattering internal standard method (hereafter, the scattering internal standard method) using the Rh-Kα–Compton scattering line intensity as an internal standard was applied. On the other hand, for analytical lines with wavelengths longer

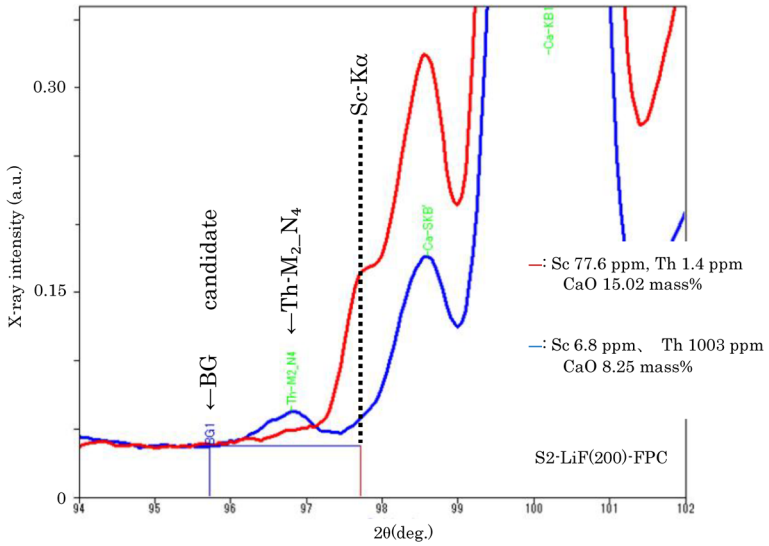

Fig. 8. Minor transition lines near the background of Sc-Kα

Table 5. List of Measurement Lines and Applied Matrix Correction Methods

Matrix correction	Compton scattering internal standard method	Absorption correction			No correction
		a)TiO_2, CaO, K_2O	b)CaO, K_2O	c)K_2O	
Absorption Edge for Major		Fe-K_{abs}	Ti-K_{abs}	Ca-K_{abs} / K-K_{abs}	
Analytical lines for major and correction	Rh-Kα Compton	Fe-Kα	Ti-Kα	Ca-Kα	K-Kα, S-Kα, P-Kα, Mg-Kα, Na-Kα
Analytical Lines for trace	Sb-Kα, Sn-Kα, Cd-Kα, Ag-Kα, Mo-Kα, Nb-Kα, Zr-Kα, Y-Kα, Sr-Kα, U-Lα, Rb-Kα, Th-Lα, Pb-Lβ1, Br-Kα, As-Kβ1, Bi-Lα, Ge-Kα, Ga-Kα, Zn-Kα, W-Lα, Cu-Kα, Hf-Lα, Ni-Kα, Yb-Lα	Co-Kα, Mn-Kα, Eu-Lα, Sm-Lα, Pr-Lβ1, Cr-Kα, Ce-Lβ1, Nd-Lα	V-Kα, La-Lα, Ba-Lα, Sc-Kα		F-Kα

Short — Wavelength — Long

(lower energy) than Fe-K_{abs}, an absorption correction was applied targeting only the absorption edges of the dominant major components (Ti-K_{abs}, Ca-K_{abs}, and K-K_{abs}). Coefficients based on a theoretical matrix correction were used as the correction factors. The correspondence between the measurement lines and their respective correction methods is shown in Table 5.

〈Scattering Internal Standard Method〉

The Compton scattering intensity is inversely proportional to the mass absorption coefficient. This scattering line is used as an internal standard line to correct for matrix effects on the analytical line. The calibration curve equations for the internal standard method are shown in Equations (1) and (2).

$$\hat{W}_i = aI_{iR} + b \tag{1}$$

$$I_{iR} = \frac{I_i}{I_{Rh-Ka-C}} \tag{2}$$

Here, $\hat{W}_i$ is the calculated value of the analyte, a is the slope of the calibration curve with respect to the intensity ratio I_{iR}, b is the intercept of the curve, I_{iR} is the intensity ratio, I_i is the intensity of the analytical line, and $I_{Rh-Ka-C}$ is the Rh-Kα-Compton intensity.

〈Absorption Correction〉

For measurement lines in the wavelength region from Fe-K_{abs} to Ca-Kα, an absorption correction is applied to reduce the influence of the absorption edges of major components (TiO_2, CaO, and K_2O). The inter-element correction formula is shown in Equation (3).

$$W_i = (aI_i + b)(1 + \Sigma \alpha_j W_j) \tag{3}$$

Here, W_j is the concentration of the coexisting element and α_j is the inter-element correction constant (theoretical matrix correction). All other symbols have the same meaning as in Equations (1) and (2).

2.5.1. Comparison of Calibration Curve Accuracy between Scattering Internal Standard Method and Absorption Correction

The accuracy (ACC) is defined as the standard deviation based on the difference between the standard and calculated values, and is calculated using Equation (4). A smaller ACC value indicates a better fit to the calibration curve.

$$ACC = \sqrt{\frac{\Sigma(W_i - \hat{W}_i)^2}{n-1}} \tag{4}$$

Here, W_i is the standard value of the analyte in the standard sample, $\hat{W}_i$ is the calculated value of the analyte, and n is the number of standard samples.

〈Example of Sr Applying the Scattering Internal Standard Method〉

In the analysis of Sr, calibration curves using the Sr-Kα line were compared for cases with no correction (Fig. 9-1), and correction by the scattering internal standard method (Fig. 9-2) and absorption correction (Fig. 9-3). The concentration range of Sr was up to approximately 1000 ppm. For the absorption correction of Sr-Kα, the correction was applied with Fe_2O_3, TiO_2, CaO, and K_2O as the primary coexisting components, as their absorption edges are dominant. The ACC without correction (Fig. 9-1) was 58 ppm, while the scattering internal standard method (Fig. 9-2) showed a significant improvement (12 ppm). Although a certain degree of improvement was also observed with an absorption correction (Fig. 9-3), the effect was not sufficient. These results indicate that in the scattering internal standard method, the Compton scattering intensity reflects the influence of not only the major components but also light elements, such as carbonate groups and carbon. Thus, it enables more accurate correction than an absorption correction using only major components, leading to the adoption of the scattering internal standard method.

〈Ba Measurements with an Absorption Correction〉

Regarding the analysis of Ba, calibration curves using the Ba-Lα line were compared with no correction (Fig. 10-1), and correction using the scattering internal standard (Fig. 10-2) and absorption correction (Fig. 10-3) methods. The concentration range of Ba was up to approximately 2500 ppm. For the absorption correction of Ba-Lα, CaO and K_2O were used as the major coexisting components that affect the absorption edge. In the case of no correction (Fig. 10-1), the ACC was 65 ppm. In contrast, with the scattering internal standard method (Fig. 10-2), the accuracy deteriorated to 180 ppm. This is because the Rh-Kα–Compton intensity used as the scattering line fluctuates significantly due to the influence of the Fe absorption edge (Fe-K_{abs}), whereas Ba-Lα is not affected by the Fe-K absorption edge. Therefore, it is inappropriate to use the Rh-Kα–Compton ratio to correct Ba-Lα. When an absorption correction was applied (Fig. 10-3), the accuracy was 37 ppm, a significant improvement compared to the uncorrected results.

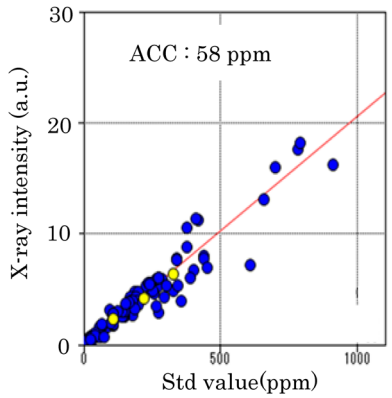

Fig. 9-1. Sr-Kα
No correction

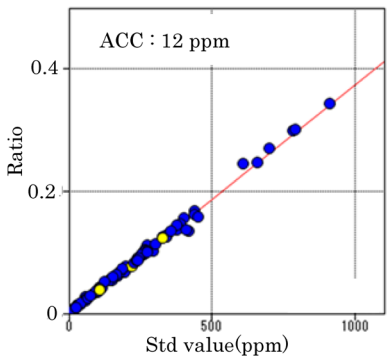

Fig. 9-2. Sr-Kα
Correction by the scattering internal standard method

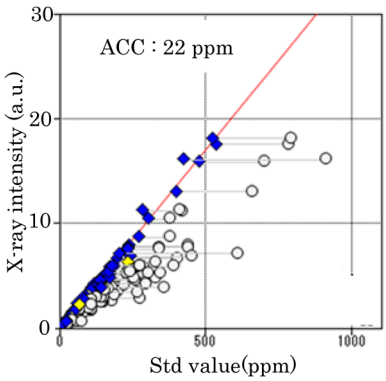

Fig. 9-3. Sr-Kα
Absorption correction

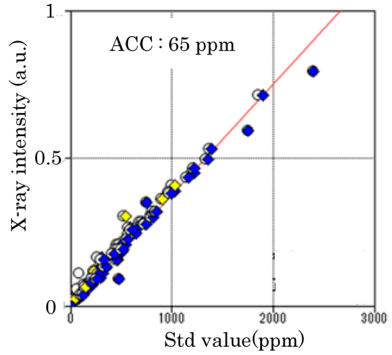

Fig. 10-1. Ba-Lα
No correction

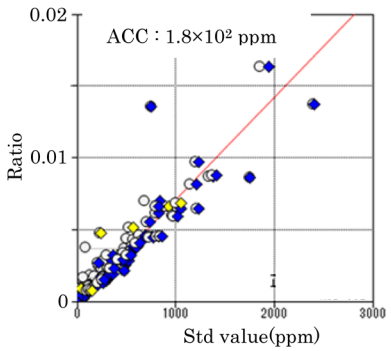

Fig. 10-2. Ba-Lα
Scattering internal standard method

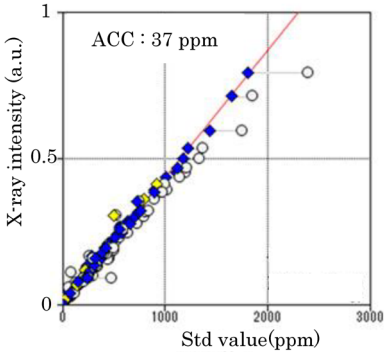

Fig. 10-3. Ba-Lα
Absorption correction

2.6. Binder Addition Correction

For samples with low pressure-moldability, a binder is added to ensure structural integrity. However, the dilution effect resulting from the addition of a binder causes a corresponding decrease in the intensity of the analytical peaks. Furthermore, for elements to which the scattering internal standard method is applied, the intensity ratio fluctuates due to a further increase in scattering intensity. All of these effects can be treated as intensity changes caused by coexisting element effects and can be corrected using an appropriate correction formula.

2.6.1. Correction Formula for Binder Addition

The weakening and fluctuations in the scattering line ratio caused by the addition of a binder are treated as part of the coexisting element effects, and the correction formula in Equation (5) is used.

$$\hat{W}_i=(aI_i+b)(1+\Sigma\alpha_jW_j-\alpha_{Binder}\bar{R}_{Binder}+\alpha_{Binder}R_{Binder}) \quad (5)$$

Here, I_i includes the ratio intensity I_{iR}, α_j is the inter-element correction constant (theoretical matrix correction), α_{Binder} is the correction coefficient for the ratio of the binder added to the sample (theoretical matrix correction), $\bar{R}_{Binder}$ is the reference binder addition ratio, R_{Binder} is the actual binder addition ratio; both ratios refer to a weight percentage (wt%). All other symbols have the same meanings as in previous equations.

Equation (5) can be simplified by combining the constant terms, as shown in Equation (6), where the term $k+\alpha_{Binder}R_{Binder}$ corrects for the influence of the deviation from the reference ratio.

$$\hat{W}_i=(aI_i+b)(1+\Sigma\alpha_jW_j+k_i+\alpha_{Binder}R_{Binder}) \quad (6)$$

$$k_i=-\alpha_{Binder}\bar{R}_{Binder} \quad (7)$$

The correction constants α_j and α_{Binder} were calculated using the fundamental parameter method implemented in the data processing system provided with the instrument. Since α_{Binder} and $\bar{R}_{Binder}$ can be set as constant terms, Equations (6) and (7) are applied in practical operation.

2.6.2. Examples

To verify the effectiveness of the binder addition ratio correction, the deviations in the quantitative values of binder-added samples were evaluated using a calibration curve established without a binder as the reference. The sample preparation conditions and criteria are shown below.

- Sample preparation conditions:
  Binder : Sample = 1 : 9 (10% addition)
  Binder : Sample = 2 : 8 (20% addition)
  Binder type: SpectroBlend® by Chemplex (Cat. No. 660, 44 µm Powder)
- Reference addition ratio: $\bar{R}_{Binder}$ = 1 : 9 (10% addition)

The results for samples prepared with 10% and 20% binder and representative binder-free samples used to create the calibration curve were compared. The differences between the X-ray analytical values after applying corrections for binder addition and those obtained under binder-free reference conditions were evaluated.

〈Sr-Kα: Calibration Curve Applying the Scattering Internal Standard Method〉

Figure 11 shows the Sr-Kα results for samples containing 10% and 20% binder plotted with the calibration curve created with binder-free samples. The Sr-Kα X-ray and scattering intensities, and Sr-Kα/scattering ratio are shown in Table 6. Since Sr-Kα has high energy and a deep analytical depth, the absorption effect on Sr-Kα is small, even when a binder (whose primary elements are C, H, N, O) is added; thus, the Sr-Kα intensity is not significantly attenuated by binder addition. In contrast, since the scattering intensity increases in inverse proportion to the mass absorption coefficient, binder addition increases the scattering intensity, leading to a significant change in the intensity ratio. After correcting for binder addition using Equation (6), the plots of the binder-containing samples fall on (or near) the binder-free calibration curve, confirming the efficacy of the correction method.

Furthermore, Table 7 shows the quantitative values obtained from the calibration curve for the same sample. Evaluating the differences (measured value minus reference) and the relative error ratios for each binder addition (10%, 20%) relative to the binder-free reference showed that all results were within a few percent, indicating the effectiveness of the correction method.

〈Case Study of Ba-Lα: Calibration Curve with Absorption Correction〉

The Ba-Lα line in the heavy-element region requires an absorption correction. Figure 12 shows a Ba-Lα calibration curve created with binder-free references samples and data for samples containing 10% and 20% binder. The X-ray intensities of Ba-Lα (Table 8) show the quantitative values obtained from the

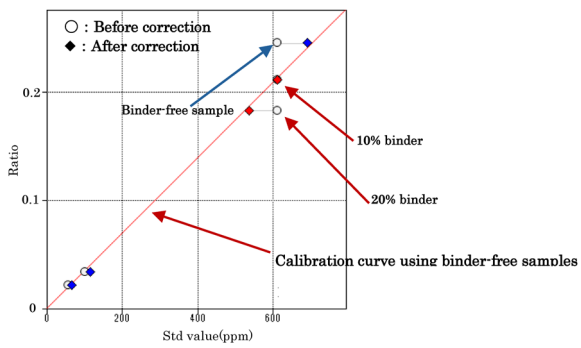

Fig. 11. Sr-Kα calibration curves for samples with and without binder

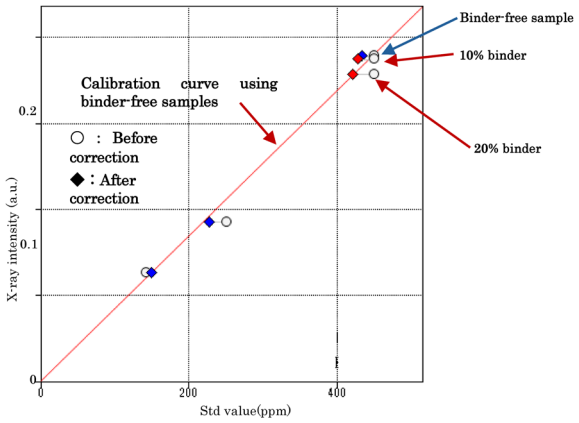

Fig. 12. Ba-Lα calibration curves for samples with and without binder

Table 6. Sr-Kα and scattering intensities, and intensity ratios for different binder additions

Binder content	Sr-Kα		Scattering line		Intensity ratio
	Intensity (kcps)	Ratio	Intensity (kcps)	Ratio	
0% (Reference)	7.0644	1	28.8549	1	0.2448
10%	7.0645	1.000	33.4282	1.1585	0.2113
20%	7.0606	0.9995	38.5990	1.3377	0.1829

Table 7. Measured Sr content and relative errors for different binder additions

Binder addition	Measured Sr content (ppm)	Difference (ppm)	Relative error (%)
0% (Reference)	623	—	—
10%	607	−16	−2.5
20%	600	−23	−3.7

Table 8. Ba-Lα intensities for different binder additions

Binder content	Ba-Lα	
	Intensity (kcps)	Ratio
0% (Reference)	0.18919	1
10%	0.18759	0.9915
20%	0.17875	0.9448

Table 9. Measured Ba content and relative errors for different binder additions

Binder content	Measured Ba content (ppm)	Difference (ppm)	Relative error (%)
0% (Reference)	469	—	—
10%	470	+1	+0.2
20%	455	−14	−3.0

calibration curve for identical samples with different binder additions. Evaluating the differences and relative errors for the samples with 10% and 20% binder reveals that all results are within a few percent, indicating the effectiveness of the correction method.

2.6.3. Considerations for Fluorine Analysis with Binder Addition

In XRF analysis, binders added to improve moldability coat the surface of powder particles, resulting in minor errors for analytical lines with high energy because X-ray absorption is low.

However, for analytical lines with low energy, the absorption effect caused by the binder significantly attenuates X-ray intensity. Consequently, the intensity decreases beyond the extent expected from dilution alone, resulting in errors that cannot be sufficiently addressed by standard corrections.

To evaluate this effect in fluorine analysis, Fig. 13 shows the results of plotting samples with 10% and 20% binder against a F-Kα calibration curve created with binder-free samples. The corresponding X-ray intensities of F-Kα are shown in Table 10. Even with corrections, the results deviate significantly from the binder-free calibration curve. The relative error increases in proportion to the binder content, reaching −13% for 10% binder and −33% for 20% binder. In the GEO-TRACE-PAK analytical package, the binder-addition correction is not sufficient for samples containing light elements like F (trace element) and reference quantitative compounds MgO and Na_2O. Therefore, the binder addition ratio should be limited to 10%, and it should be noted that the quantitative values obtained under this condition tend to be approximately 10% lower than the true values.

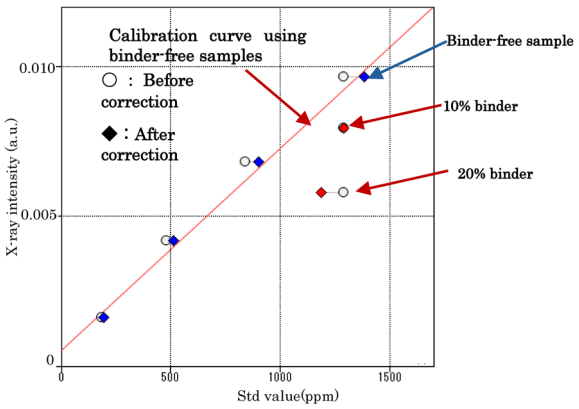

Fig. 13. F-Kα calibration curves for samples with and without binder

Table 10. F-Kα intensities for different binder contents

Binder content	F-Kα	
	Intensity (kcps)	Ratio
0% (Reference)	0.00966	1
10%	0.00796	0.8240
20%	0.00580	0.6004

Table 11. Measured F contents and relative errors for different binder contents

Binder content	Measured F content (ppm)	Difference (ppm)	Relative error (%)
0% (Reference)	1262	—	—
10%	1101	−161	−12.8
20%	848	−414	−32.8

2.7. Summary of GEO-TRACE-PAK Measurement Lines, Optical Conditions, and Inter-element Correction Methods

Table 12 summarizes the measurement lines, optical conditions, and inter-element correction methods used in this analytical package, as described in this section.

3. Analysis Examples Using GEO-TRACE-PAK

Quantitative analysis was performed using geological reference materials from IGGE (GSR-4, GSR-5, GSR-10) and CANMET (SY-3) as analytical samples. For some samples, a binder was added to improve molding. The analytical results for trace elements, including rare-earth elements, are shown in Table 13. Furthermore, samples from KIGAM (Korea Institute of Geoscience and Mineral Resources; KB-1, KGB-1, KD-1, KT-1) were similarly analyzed and the results are presented in Table 14. For all samples, the analysis results show good agreement with published certified or literature values, confirming that XRF analysis using this package provides sufficient precision and accurate results.

4. Summary

In this study, we evaluated XRF trace-element analysis using GEO-TRACE-PAK, which features pre-installed optimized calibration curves developed from approximately 110 diverse standard materials, primarily rocks and ores. Because this package comes pre-configured with various parameters, including optimized optical conditions and inter-element corrections, it enables users to begin analysis immediately after instrument installation. The user can simply install the analytical application and measure a few monitor samples for sensitivity calibration, without the need to purchase expensive standard materials. Verification using geological reference materials confirmed that the analytical values obtained by this method are in good agreement with published certified and literature values, demonstrating sufficient analytical precision and reliability. Combining ease of implementation with high practicality, GEO-TRACE-PAK is expected to be widely utilized as a valuable analytical method for geological sample analysis.

Table 12. Summary of measurement lines, optical conditions, and inter-element correction methods in the GEO-TRACE-PAK analytical package

<table>
<tr><td rowspan="2">Matrix correction</td><td colspan="4" rowspan="2">Compton scattering internal standard method</td><td colspan="8">Absorption correction</td><td colspan="3" rowspan="2">No correction</td></tr>
<tr><td colspan="3">a)TiO$_2$, CaO, K$_2$O</td><td colspan="4">b)CaO, K$_2$O</td><td>c)K$_2$O</td></tr>
<tr><td>Absorption Edge for Major</td><td></td><td></td><td></td><td>Fe-K$_{abs}$</td><td></td><td></td><td>Ti-K$_{abs}$</td><td></td><td></td><td></td><td>Ca-K$_{abs}$</td><td>K-K$_{abs}$</td><td></td><td></td><td></td></tr>
<tr><td>Analytical lines for major and correction</td><td></td><td>Rh-Kα Compton</td><td></td><td></td><td></td><td>Fe-Kα</td><td></td><td></td><td></td><td>Ti-Kα</td><td></td><td>Ca-Kα</td><td>K-Kα</td><td>S-Kα P-Kα</td><td>Mg-Kα Na-Kα</td></tr>
<tr><td>Analytical Lines for trace</td><td>Sb-Kα Sn-Kα Cd-Kα Ag-Kα</td><td></td><td>Mo-Kα Nb-Kα Zr-Kα Y-Kα Sr-Kα U-Lα Rb-Kα Th-Lα Pb-Lβ1 Br-Kα As-Kβ1 Bi-Lα Ge-Kα Ga-Kα</td><td>Zn-Kα W-Lα Cu-Kα Hf-Lα Ni-Kα Yb-Lα</td><td>Co-Kα</td><td></td><td>Mn-Kα Eu-Lα Sm-Lα Pr-Lβ1 Cr-Kα Ce-Lβ1 Nd-Lα</td><td>V-Kα</td><td>La-Lα</td><td>Ba-Lα</td><td>Sc-Kα</td><td></td><td></td><td></td><td>F-Kα</td></tr>
<tr><td>Primary X-ray Filter</td><td>Ni400</td><td>Al25</td><td>Ni40</td><td colspan="2">Al125</td><td>Al25</td><td colspan="3">Al125</td><td colspan="4">Al25</td><td colspan="2">Be30 or Out</td></tr>
<tr><td>Analysis Crystal</td><td colspan="7">LiF(220)</td><td colspan="6">LiF(200)</td><td>Ge</td><td>RX26</td></tr>
<tr><td>Detector</td><td colspan="8">SC</td><td>FPC</td><td>SC</td><td colspan="5">FPC</td></tr>
<tr><td>Divergent Slit</td><td colspan="11">S2</td><td>S4</td><td colspan="3">S2</td></tr>
</table>

Table 13. Analytical results for IGGE (GSR-4, GSR-5, GSR-10) and CANMET (SY-3) samples

Ele.	Unit	GSR-4 (Sandstone)		GSR-5 (Shale)		GSR-10 (Gabbro)		SY-3 (Syenite)	
		without binder		without binder		5% binder		10% binder	
		XRF*	recommended	XRF*	recommended	XRF*	recommended	XRF*	recommended
Sc	ppm	4.9±0.6	4.2	21±1	18.5	20±1	22.5	2.8±0.8	6.8
V	ppm	34±0.9	33	87±1	87	773±3	768	36±1.2	50
Cr	ppm	26±3	20	128±5	99	18±5	14.5	14±4	11
Mn	ppm	155±7	155	184±8	173	1361±23	1498	2328±29	2483
Co	ppm	9.6±1.1	6.4	29±2	21	100±3	93	16±2	8.8
Ni	ppm	17±1	16.6	44±2	37	91±3	69	21±2	11
Cu	ppm	19±1	19	44±1	42	32±2	28.3	13±1	17
Zn	ppm	19±1	20	54±1	55	122±2	118	248±2	244
Ga	ppm	5.3±0.7	5.3	23±1	26	22±1	23.7	27±1	27
Ge	ppm	<1	1.16	4.1±0.4	3.1	<1	1.06	<1	1.4
As	ppm	8.9±1.6	9.1	<5	1.4	<5	0.21	23±3	18.8
Br	ppm	<0.7	1	<1	0.4	<1	0.32	<1	0.646
Rb	ppm	29±1	29	212±1	205	3.7±0.6	4.79	208±1	206
Sr	ppm	59±1	58	94±1	90	664±2	612	305±1	302
Y	ppm	24±1	21.5	31±1	26	7.5±0.7	4.9	705±2	718
Zr	ppm	204±1	214	98±1	96	16±1	29	346±1	320
Nb	ppm	4.9±0.4	5.9	14±1	14.3	5.1±0.7	9.3	136±1	148
Mo	ppm	<1	0.76	<1	0.35	<1	0.094	<1	1
Ag	ppm	<2	0.062	<2	0.047	<2	0.05	<2	1.5
Cd	ppm	<2	0.06	<2	0.033	<2	0.09	<2	0.203
Sn	ppm	<1	1.1	5.7±1.0	2	18±2	0.89	17±1	6.5
Sb	ppm	<2	0.6	<2	0.18	<2	0.04	<2	0.31
Ba	ppm	147±3	143	465±4	450	54±6	86.2	439±4	450
La	ppm	21±2	21	67±2	62	<3	1.71	1355±7	1430
Ce	ppm	58±6	48	144±7	109	<11	4.2	2646±19	2230
Pr	ppm	<8	5.4	19±7	13.6	<8	0.84	252±10	223
Nd	ppm	24±3	21	59±4	48	<6	4.1	788±8	670
Sm	ppm	6.9±1.2	4.7	12±4	8.4	<2	1.22	144±6	109
Eu	ppm	<1	1.02	1.4±0.5	1.7	2.4±0.7	0.74	8.9±0.8	17
Yb	ppm	<3	1.9	<3	2.6	<3	0.36	59±2	62
Hf	ppm	2.7±1.2	6.6	2.9±1.4	2.9	<2	0.65	12±2	9.7
W	ppm	<1	1.2	<1	0.79	<1	0.1	7.1±2	1.1
Pb	ppm	7.0±0.8	7.6	6.9±0.9	8.7	<1	5.16	144±2	133
Bi	ppm	<2	0.18	<2	0.23	<2	0.04	<2	0.8
Th	ppm	7.0±0.6	7	13±1	12.8	<1	0.28	1023±3	1003
U	ppm	5.3±0.5	2.1	2.8±0.6	1.5	2.6±0.9	0.086	681±2	650
F	ppm	300±65	183	1061±89	1290	148±84	60	6285±146	6960

*The errors of the XRF analytical values are expressed as the standard deviation (1σ) obtained from the measured results.

Table 14. Analytical results for KIGAM samples (KB-1, KGB-1, KD-1, KT-1)

Ele.	Unit	KB-1 (Basalt)		KGB-1(Gabbro)		KD-1(Diorite)		KT-1(Trachyte)	
		without binder		without binder		without binder		without binder	
		XRF*	Literature[a)]	XRF*	Literature[a)]	XRF*	Literature[a)]	XRF*	Literature[a)]
Sc	ppm	16±1	19.4, 23	20±1	25, 27.3	18±0.8	15.3, 22	<1	0.67, 5.1
V	ppm	152±2	151	160±2	104	123±2	106	8.8±0.9	8.05
Cr	ppm	313±7	281–304	84±5	69–85	62±4	54.3–62	15±3	6
Mn	ppm	1165±20	1217	919±18	1001	974±18	1008	1677±23	1860
Co	ppm	53±2	24–54	29±2	26–29	25±2	20.1–45	4.0±1.1	0.4–7
Ni	ppm	186±3	164–193	28±1	22–26	20±1	16–24	2.6±1.1	1.3
Cu	ppm	64±2	—	47±1	—	37±1	—	<3	—
Zn	ppm	80±1	73, 87	73±1	80, 86	67±1	63, 79	95±1	107
Ga	ppm	19±1	—	18±1	—	18±1	—	23±1	—
Ge	ppm	<1	—	<1	—	<1	—	<2	—
As	ppm	<5	—	<5	—	<5	—	<5	—
Br	ppm	<1	—	<1	—	<1	—	<1	—
Rb	ppm	22±1	19.3–26	62±1	55–65	72±1	66–75	127±1	115–130
Sr	ppm	530±2	488–518	437±1	412–431	451±1	432–444	719±2	697–733
Y	ppm	24±1	—	28±1	—	28±1	—	43±1	—
Zr	ppm	157±1	153–164	178±1	155–199	181±1	171–204	712±1	543–737
Nb	ppm	26±1	—	6.8±0.5	—	6.9±1	—	125±1	—
Mo	ppm	<1	—	<1	—	<1	—	2.4±0.2	—
Ag	ppm	<2	—	<2	—	<2	—	<2	—
Cd	ppm	<2	—	<2	—	<2	—	<2	—
Sn	ppm	9.4±1.2	—	7.9±1.1	—	6.7±1.1	—	6.9±1.0	—
Sb	ppm	<2	—	<2	—	<2	—	<2	—
Ba	ppm	293±4	113–275	529±5	424–557	551±5	443–647	1150±6	905–1450
La	ppm	20±2	21	27±2	32	28±2	32	93±2	99
Ce	ppm	48±7	33–42	65±7	51–66	64±7	47–62.8	185±8	174–184
Pr	ppm	13±7	6	9.8±6	7	<7	7.7	24±6	16.9
Nd	ppm	23±4	27	32±4	31	29±4	40	69±4	82
Sm	ppm	<4	4.54–4.97	5.3±4	5.9	6.4±4	5.8	10±4	11
Eu	ppm	1.8±0.6	1.7	1.4±0.6	1.4	1.4±0.6	1.5	1.2±0.6	3.1
Yb	ppm	<3	2.1	<3	2.8	<2.9	2.8	3.8±1.1	4.3
Hf	ppm	4.9±1.8	3.6	5.4±1.6	4.9	5.8±1.6	5	12±9	16
W	ppm	<1	—	<1	—	<1	—	<2	—
Pb	ppm	3.0±1.1	—	12±1	—	15±1	—	6.4±0.9	—
Bi	ppm	<2	—	<2	—	<2	—	<2	—
Th	ppm	2.7±0.9	2.1–2.7	6.8±0.8	4.9–7.1	8.4±0.8	8.3, 8.9	16±1	14.6–17
U	ppm	2.5±0.7	0.7	3.1±0.6	1.1	3.1±0.6	1.58	4.2±0.6	4
F	ppm	413±73	—	548±79	—	536±77	—	228±61	—

*The errors of the XRF analytical values are expressed as the standard deviation (1σ) obtained from the measured results.

a) Naoki Shirai et al., Multi-element analysis of Korean geological reference materials by INAA, ICP-AES and ICP-MS. *Journal of Radioanalytical and Nuclear Chemistry*, **303**, 1367–1374. 2015.

References

(1) Rigaku Corporation: Trace Element Analysis in Geological Samples by Pressed Powder Method Using GEO-TRACE-PAK, XRF Application Note, XRF 1099

